International Journal of Thin Films Science and Technology

http://dx.doi.org/10.18576/ijtfst/080208

Ion Source Plasma Parameters Measurement using Langmuir Probe

Hikmat A. Hamad[*] *and Haitham M. Farok*

Department of Mathematics and Applied Sciences, college of Arts and sciences, University of Abu Dhabi, United Arab Emirates.

Received: 3 Mar. 2019, Revised: 2 Apr. 2019, Accepted: 12 Apr. 2019

Published online: 1 May 2019

Abstract: In this work, we present the experimental results of plasma parameters using a Freeman type ion source, such as electron number density n_e, plasma electron temperature T_e, floating potential V_f, and plasma potential V_S. The measurements of these basic parameters of pure *Ar* plasma were done with a cylindrical Langmuir probe situated perpendicular to a relatively weak magnetic field, B = 20 mT and were performed under constant low *Ar* pressure 4.6×10^{-3} mbar. Different methods were implemented to calculate the electron and ion densities. We have concluded that some of these methods are subjected to significant inaccuracy, mainly due to the uncertainty of the plasma potential location. However, It has been recognized that the plasma ion density $n_i = 1.46 \times 10^{14}$ m^{-3} found in this experiment using the ion current saturation part is the most reliable among the other values found, using the standard procedures from the electron retardation region (classic Langmuir method) and the electron saturation region of the measured probe I–V characteristic. The results of calculations confirm the validity of the Langmuir's orbital-motion-limited theory for low pressure plasma and low value of the magnetic field.

Keywords: Freeman Ion source; Langmuir probe; Plasma potential; Electron temperature; Electron density.

1 Introduction

The ion source is one of the most important part in equipment used for ion implantation and other processes like nuclear fusion or electromagnetic separators (EMIS). In this work a modified Freeman ion source, used for ion sputtering, is designed and constructed to be installed in the ion implantation unit. The choice of this ion source was based on its remarkable success in the semiconductor industry employing ion implantation techniques. The detailed and technical description of the design and fabrication of the main parts of the freeman type - ion source and the study of its arc characteristics can be found in reference [1]. One of the key part of any ion source using plasma as a source for generating ions, is the plasma parameters; such as electron temperature (T_e), electron density (n_e), and floating potential (V_f). Langmuir probe is considered the most suitable tool for the determination of these parameters due to its simplicity in measuring their local values. Langmuir probe can be used for the direct measurement of plasma potential and current voltage (I–V), which can be utilized for the measurement of the electron energy distribution function (EEDF) [2-5]. In this work we have used the Langmuir diagnostic technique to determine the plasma parameters in low-temperature and low-pressure argon plasma of the Freeman ion source. A typical I–V curve is characterized by three main regions of the ion saturation; the region where $V < V_f$, the region where $V_p < V_S$ (the electron retardation) and the region $V_p > V_s$, (the electron saturation) as shown in Fig.1. Where V_f , is the floating potential at which the electron and the ion current are equal, $I_e = I_i$ and V_P is the plasma or space charge potential. Each part of the (I–V) curve, carries some information about the plasma parameters [6].

It has been well established in the literature, that when the electrons in the plasma have a Maxwellian distribution with temperature T_e, then the electron current I_e will follow an exponential function of the probe voltage V_P up to the space or plasma potential V_S, which is normally called the retarding region. At V_S the electron current I_e will reach the saturation region at which the slope $|dI/dV|$ will be maximum. The space potential, *Vs*, of the plasma can be obtained from the position of the knee of the electron saturation portion of the full (I–V) characteristic as the probe bias voltage changes from electron retarding to electron accelerating. This can be done in two ways. First, by finding the intersection of the straight lines of the semi-

[*]Corresponding author E-mail: hikmat.hamad@adu.ac.ae

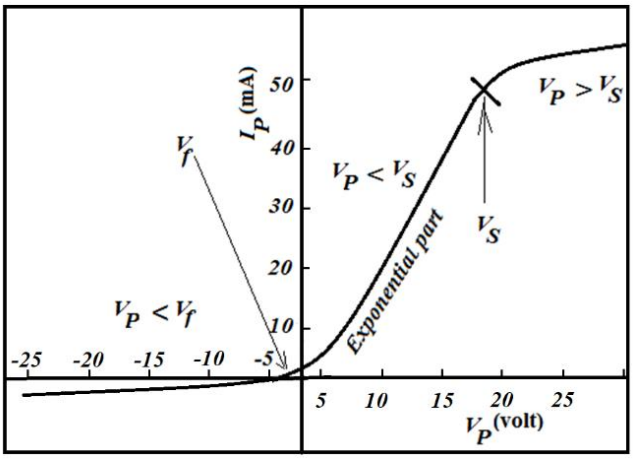

Fig.1: Typical Langmuir (I –V) characteristics, V_S, V_f and V_P are the space or plasma potential, floating potential and probe potential respectively.

log plot of the electron current versus probe voltage. Secondly, by finding the maximum value of the first derivative $|dI_P/dV|$, which has been adopted in this work, or by using the zero-cross of the second derivative of the total current of the (I–V) probe characteristics [7-10]. Previous published works [11-18] show that above the floating potential V_f, the electron current I_e as a function of the probe potential V_p is given by:

$$I_e = I_{esat}\, exp\left[\frac{e(V_p - V_S)}{k_B T_e}\right] \qquad Vp < V_S \qquad (1)$$

Where I_{esat} is the saturation electron current and is given by;

$$I_{esat} = en_e A_p \left(\frac{k_B T_e}{2\pi m_e}\right)^{1/2} \qquad (2)$$

$$I_e = en_e A_p \left(\frac{k_B T_e}{2\pi m_e}\right)^{1/2} exp\left[\frac{e(V_p - V_S)}{k_B T_e}\right] \quad Vp < V_S \qquad (3)$$

Where I_e, is the electron current, n_e is the electron density, A_p the collection probe surface area, T_e the electron temperature, m_e and e are the electron mass and charge, respectively.

The inverse of the gradient of a plot of LnI_e versus the applied probe voltage, V_P, yields the electron temperature:

$$T_e = \left[\frac{dLnI_e}{dV_p}\right]^{-1} \qquad (4)$$

The expression for the current collected by a cylindrical probe having a Maxwellian - electron velocity distribution in the electron saturation region $V_P > V_S$ [19, 20] is given by:

$$I_e = en_e A_p \left(\frac{k_B T_e}{2\pi m_e}\right)^{1/2} \frac{2}{\sqrt{\pi}} \left[1 - \frac{e(V_p - V_S)}{k_B T_e}\right]^{1/2} \quad V_P > V_S$$

The increase in the electron current I_e in the saturation region is due to sheath expansion effects. In many experiments, it is not easy to see the electron saturation region, which require higher probe biasing voltage. Equation (5) can be rewritten as:

$$I_e^2 = \frac{2e^2 n_e^2 A_P^2}{\pi m_e}[k_B T_e + e(V_P - V_S)] \quad V_P > V_S \ (6)$$

Equation (6) shows a linearity between the square of electron current (I_e^2) and the probe potential V_P. The derivative of I_e^2 with respect to V_P yields:

$$\frac{dI_e^2}{dV_P} = \frac{2A_P^2 e^3}{\pi m_e} n_e^2$$

$$n_e \cong \frac{1.87\times10^{13}}{A_{P\,(m^2)}} \sqrt{\left(\frac{dI_e^2}{dV_p}\right)} \quad m^{-3} \quad V_P > V_S \qquad (7)$$

Equation (7) can be used to find the electron density n_e within the electron saturation part. The probe current I_P is the sum of the electron and ion current collected by the probe ($I_P = I_e + I_i$). The ion saturation part of the characteristic graph is used to determine the ion density n_i. Langmuir's orbital-motion-limited (OML) theory provides a simple formula for ion current [16], which was summarized by Chen [17, 18], and given by the following approximate formula for saturation ion current I_i drawn by a negatively biased cylindrical probe:

$$I_i = n_i e A_P \left(\frac{k_B T_e}{2\pi m_i}\right)^{1/2} \frac{2}{\sqrt{\pi}} \left[\frac{e(V_S - V_P)}{k_B T_e}\right]^{1/2} \qquad (8)$$

$$I_i^2 = \frac{2A_p^2\, e^3}{\pi^2 m_i} n_i^2 \ (V_S - V_P) \qquad (9)$$

Where, m_i is the ion mass. Equation (9) is a very useful formula, since it can be used to determine n_i without a prior determination of T_e. In the absence of any electron current I_e the square of the probe current I^2_p should be a linear function of the probe potential V_p and the derivative of I_i^2 with respect to V_p yields:

$$\frac{dI_i^2}{dV_p} = -\frac{2A_p^2\, e^3}{\pi^2 m_i} n_i^2 \qquad (10)$$

or

$$n_i = \sqrt{\frac{\pi^2 m_i}{2A_p^2 e^3}\left(-\frac{dI_i^2}{dV_p}\right)} \qquad (11)$$

or

$$n_i \cong \frac{1.42\times10^{15}}{A_{P\,(m^2)}} \sqrt{m_i\,(\text{amu})\left(-\frac{dI_i^2}{dV_p}\right)} \quad m^{-3} \qquad (12)$$

Equation (8) fails if collisions occur within very thick sheath and is only valid for the limiting case for low Debye

length, in which the sheath thickness is small in comparison with probe diameter, where:

$$\lambda_D = \left(\frac{\varepsilon_o\, kT_e}{e^2 n_e}\right)^{1/2} \quad (13)$$

λ_D denotes the Debye length, n_e the electron density, T_e the electron temperature, ε_o = 8.85 × 10^{-12} N.m^2/C^2, the permittivity of free space, k = 1.38 × 10^{-23} J/K and r_p is the probe radius. A handy formula for the Debye length is:

$$\lambda_D(m) = 7.44 \times 10^3 \sqrt{\frac{T_e(eV)}{n_e(m^{-3})}} \quad (14)$$

The positive ion density n_i can also be calculated using the measured probe current in the region where $V_P < V_f$. The experimental work of Chen [21] shows that saturation ion currents I_i for cylindrical probes in the 10^{10} – 10^{12} cm^{-3} density range tend also to follow an $I_i \sim V_P^{3/4}$ (Child–Langmuir law, where V_P is the probe voltage). Extrapolating to the floating potential V_f , which is easily measured, one can obtain an estimate of the ion (or electron) current at V_f . The $I_i \sim V_P^{3/4}$ is indicative of the Child– Langmuir (CL) law for plane electrodes. If one assumes that the CL law (neglecting the cylindrical curvature) gives the sheath thickness, then the collection area expands as $V_p^{3/4}$, giving rise to the observed shape of the (I–V) curve. For plasmas having low electron density, the floating potential method (FP-CL) cannot provide a good estimation of the positive ion density because the sheath length becomes large. At low densities, the I_i^2 approach fits better to a straight line compared to the $I_i^{4/3}$ approach, suggesting that some ion orbiting is taking place [21]. The floating potential V_f, can also be used to determine the plasma space potential, VS and the electron temperature, Te using the following relation [11, 13-15]:

$$V_f = V_S + \left(\frac{k_B T_e}{e}\right)\left[\ln\left(0.6\sqrt{\frac{2\pi m_e}{m_i}}\right)\right] \quad (15)$$

For *Ar* plasma working gas, where m_i = 6.68 × 10^{-26} kg and m_e = 9.1 × 10^{-31} kg, Eq.(15) can be simplified to:

$$V_S = V_f + 5.19\, T_{eV} \quad (16)$$

This shows that the plasma potential V_s is higher than the floating potential V_f by an amount of ~5.19T_{eV} for *Ar*-plasma, where T_{eV} is expressed in electron volts. For cylindrical probes, there is a geometrical correction, which lowers the value of 5.19 T_{eV} to a value between 4T_{eV} and 5T_{eV}, depending on the ratio of probe radius (r_P) to Debye length (λ_D) [14].

The influence of the magnetic field on the probe measurement in the collision-free case can be effective depending upon the parameter $\beta = r_P/r_{Le}$, where r_{Le} is the mean Larmor radius for electron, which is given by:

$$r_{Le} \approx \frac{3.0\, x10^{-6}}{B(Tesla)}\sqrt{T_e(eV)} \quad (17)$$

For weak magnetic field, *B*, the influence of the magnetic field on the results is small and can be neglected [22].

2 Experimental Details

The arc chamber is a parallelepiped vessel having the dimensions 49 × 44 × 72 (mm) with a cylindrical inner surface of 22 mm in diameter and is made of graphite as shown in Fig. 2a. A tantalum filament rod, of 120 mm in length and 2.3 mm in diameter, fixed axially in the arc chamber parallel to the extraction slit at a distance of 4 mm from it, as this distance does not appear to be critical. An ion outlet extraction slit, having the dimensions 1.45 mm × 43 mm, was cut parallel to the axis of the cylindrical chamber. Two circular apertures of 6 mm in diameters were drilled on both sides of the chamber. The first aperture was used as an *Ar*-gas feeding tube and the second one provided an access for insertion of a rod of tantalum into the arc chamber for plasma diagnostics purposes. This rod was used in this experiment as a single Langmuir probe and positioned perpendicular to the magnetic field. It was made of tantalum 2.3 mm in diameter and inserted inside the arc chamber such that the length of the tip of the probe exposed in the plasma was about 3 mm with a surface area of 25.83 mm^2. The probe was well insulated using ceramic beads to avoid any fake probe current collection and it was electrically connected to a variable stabilized power supply capable of biasing the probe at various positive and negative voltages relative to the plasma as shown in Fig. 2b. The operating biased probe voltage to be used for the (I–V).

measurement was in the range of –30 V to +30 V.

The vacuum system used consists of two stages of evacuation, a rotary pump and a turbo molecular pump, as shown in Fig. 2c. Experimentally, it was found that the arc was struck when the pressure inside the vacuum chamber reached a value in the 10^{-4} mbar range. In operating the ion source, the vacuum system was turned on until the pressure inside the vacuum chamber reached a value of the order of 10^{-6} mbar.

3 Results and Discussion

3.1 Electron Temperature Te and Space Potential VS Measurement of Ar Plasma.

Figure 3a shows sample of the raw data collected of the Langmuir probe characteristics using *Ar*-plasma. The (I–V) characteristics clearly shows the three distinguished

regions, the electron-current saturation I_{es}, retarding region and the ions saturation region I_{is}. The most

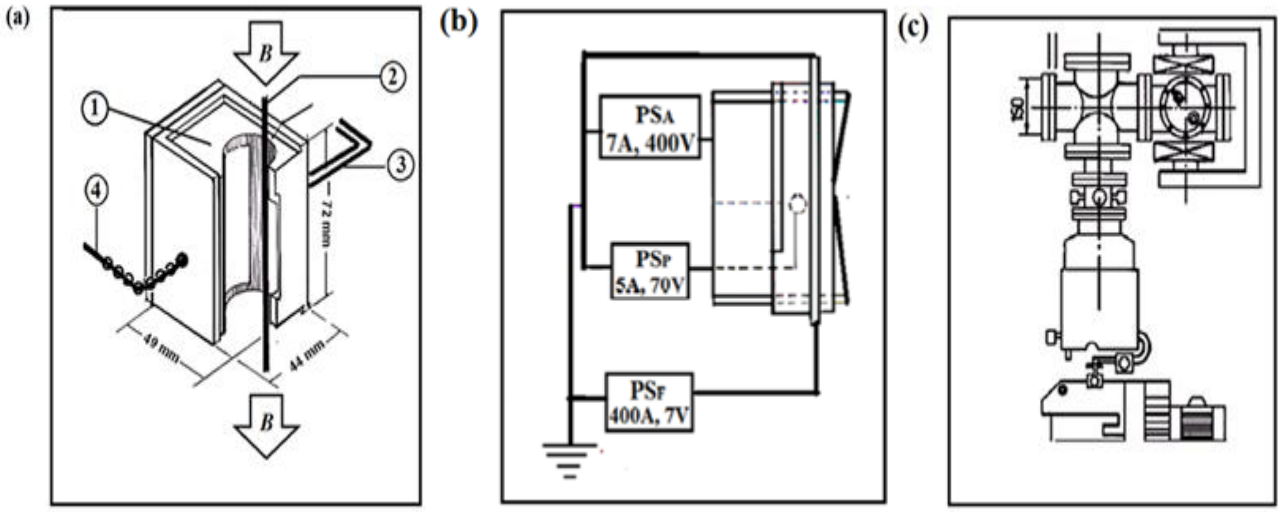

Fig. 2: (a) A schematic diagram of the cross sectional view of the arc chamber: 1) Arc chamber, 2) Filament, 3) Argon gas tube, 4) Tantalum rod threaded with ceramic beads. **(b)** Schematic diagram of the electrical circuit of the ion source. **(c)** Shows the system and vacuum chamber with the ion source electromagnet.

apparent feature of the curve is the round curved knee. It is much easier to understand the full (I–V) characteristic, if the ion and electron current contributions are discussed and analyzed separately.

The plot of $\ln I_e$, which is the net electron current collected by the probe or $\ln|I_p - I_{is}|$, against the probe potential, V_P, is shown in Fig. 3b. The figure shows a nearly linear portion up to the rounding of the knee at which both I_{es} and the space or plasma potential V_S can now be easily determined as the coordinates of the intersection (V_S, I_{es}) of the two asymptotic straight lines drawn, one parallel to the curve above the knee ($V_P > V_S$) and the other parallel to the sloping part ($V_P < V_S$). The intersection of the two lines occurs approximately at $V_S \cong 7.5$ V and $I_e \cong 110$ µA. The plasma potential found using this way is somewhat higher than the true plasma potential, *Vs* found at $d^2I/dV^2 = 0$. Similar observation was noticed by Godyak and Alexandrovich [8]. From Fig. 4, it was found, by differentiating the probe current, I_P with respect to the probe voltage V_P, that the value $V_S \cong 6.1$ V and $I_e \cong 80$ µA corresponds to the maximum of dI_P/dV_P or $d^2I_P/dV^2_P = 0$.

The slope of the linear part of Fig. 3b represents the reciprocal of the electron temperature times a universal constant according to Eq. (4). An accurate determination of the value of T_e depends upon an accurate subtraction of the ion current from the probe current I_P. Thus, to get the correct I_e, we have subtracted the saturated ion current, I_{is} from the total probe current collected. Figure 3c shows the results between $V_P = 0$ and $V_P = 6.15$ V, and it is obvious that there is a slight difference between the two lines. The slope of the uncorrected one is a little bit lower and therefore, corresponds to a higher electron temperature, T_e. It is also clear from the same figure, that the correction affects only the high-energy tail of the electron distribution. According to this temperature fit, the inverse temperature is approximately 0.402, which leads to $T_e \cong 2.48$ eV by using Eq. (4). Figure 3a shows that $V_f = -2.25$V and knowing that $T_e = 2.48$ eV, then the plasma potential V_S can be calculated using Eq. (16); $V_s = V_f + 5.19T_{eV}$. It is clear that $V_S \cong 10.67$ V, which is higher than the experimental value $V_S \cong 6.1$ V as it was estimated from Fig 4. However, this experimental value can be approximately found, if we use Eq. (16) with a factor value of 3.35 instead of 5.19, we get $V_S \cong 6.1$ V, which is in agreement with our experimental result found in Fig. 3b, within the experimental error in finding V_S. Using values of $T_e = 2.48$ eV, $B = 20$ mT and $r_p = 1.15$ mm, we can find the Larmor (r_{Le}) radius for the electron by employing Eq. (17). The calculations show that $r_{Le} \cong 0.24$ mm and $\beta = r_p / r_{Le} \approx 4.8$, which indicates that the effect of the magnetic field has a little influence on the results extracted from Langmuir probe characteristics and may be a correction for the magnetic effect is required in the evaluation of the plasma parameters. For more discussion of the influence of the magnetic field on probe measurement one can refer to the work given by Tichy [22]. Figure 3d is an example of the corrected electron current I_e plotted against the probe voltage V_P within the retarding region. It is fitted to an exponential function up to the space potential V_S and the curve indicated that the electrons have Maxwellian distribution, in agreement with Eq. (1) relationships.

3.2 Electron Density Measurement ne of Ar plasma

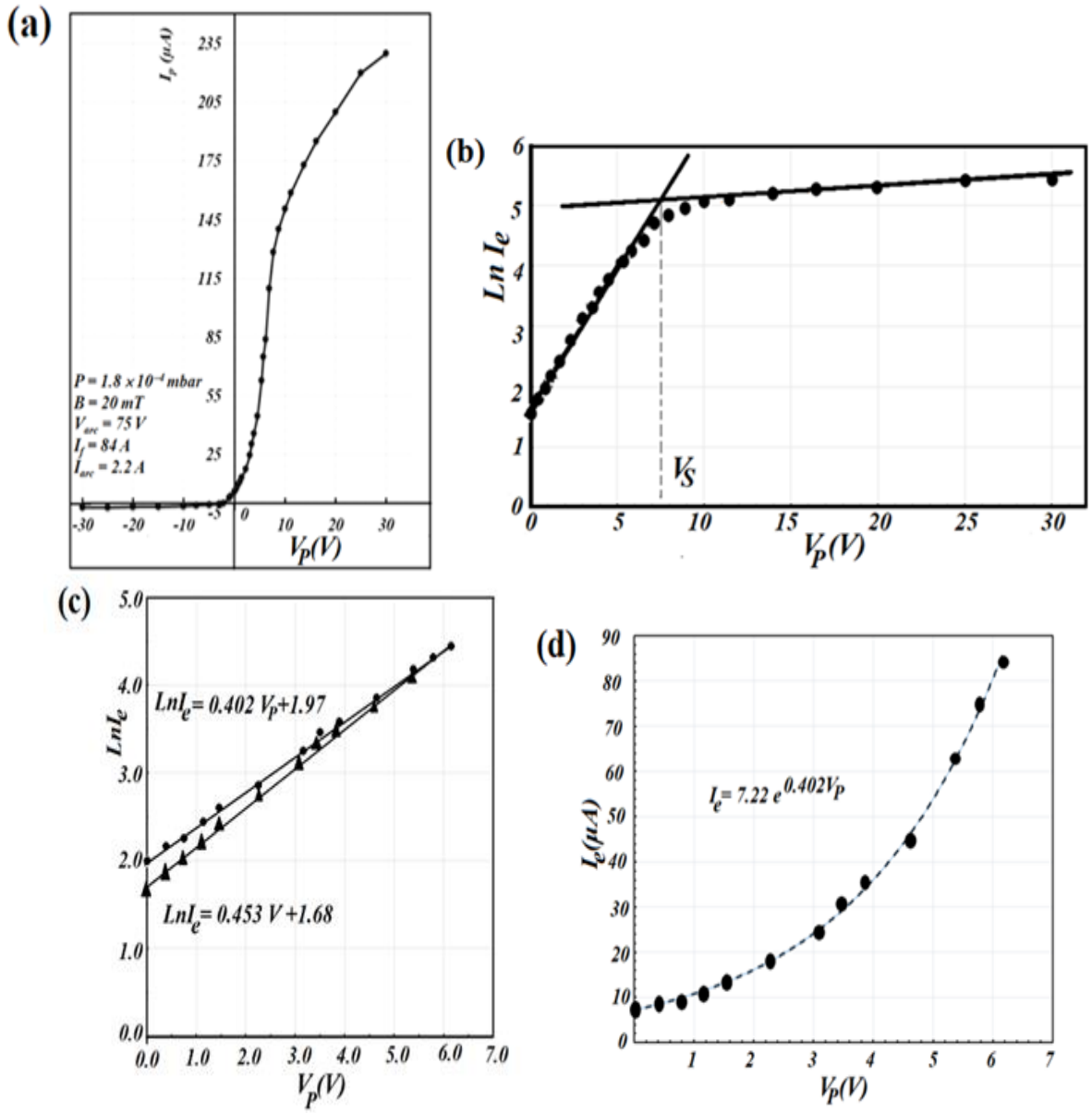

Fig. 3: (a) $I_P - V_P$ characteristics of Langmuir probe for *Ar*- plasma. **(b)** Semi- log of the $I-V$ characteristics of Langmuir probe for *Ar*- plasma wit correction showing the cross lines at **(c)** Semi- log of the $I-V$ characteristics of Langmuir probe for *Ar*- plasma with and without correction up to the knee voltage. **(d)** Exponential fitting for corrected I_e vs probe voltage V_P.

Equation (2) can be used to calculate the electron density, n_e, at the space potential, V_S. The substitution of following values; $I_e\ (V_S) \cong 80$ μA at $V_P = V_S$, $T_e = 2.48$ eV, $A_p = 2\pi r_P L + \pi r^2_P = 25.83 \times 10^{-6}$ m^2, $e = 1.60 \times 10^{-19}$ C, $m_e = 9.1 \times 10^{-31}$ kg, in this equation yields an estimated electron density of $n_e \cong 7.4 \times 10^{13}$ m^{-3} or $n_e \cong 7.4 \times 10^{7}$ cm^{-3}. This value depends exponentially on *Vs*, and therefore it is might be subjected to an error arising from the uncertainty in the determination of *Vs* [21]. Also, this value of n_e may be subjected to an error due to the influence of the magnetic field on the electron part of the I–V characteristics [9, 10], in spite of the relatively low value of the magnetic field used in this work.

3.2.2 Electron Saturation Current I_{es}

An attempt to estimate the electron density n_e using the electron saturation region was done, but the results were much lower than expected in comparison with the calculated value above, and with the value found using the ion saturation region, which will be discussed later below. Figure 5 shows a linear fitting of I^2_{es} as a function of the probe voltage V_P. Using Eq. (7) with the area of the probe $A_P = 25.83 \times 10^{-6}$ m^2, $e = 1.60 \times 10^{-19}$ C, $m_e = 9.1 \times 10^{-31}$

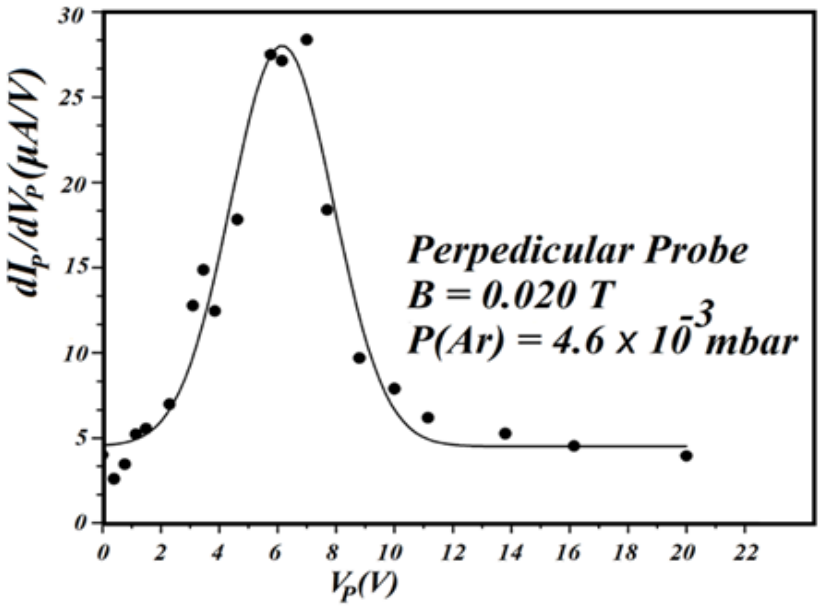

Fig.4: Fitted line of the first derivative dI_P/dV_P of the experimental $I-V$ curve in a magnetized *Ar*- plasma as a function of the probe voltage for Langmuir probe oriented perpendicular to the magnetic field.

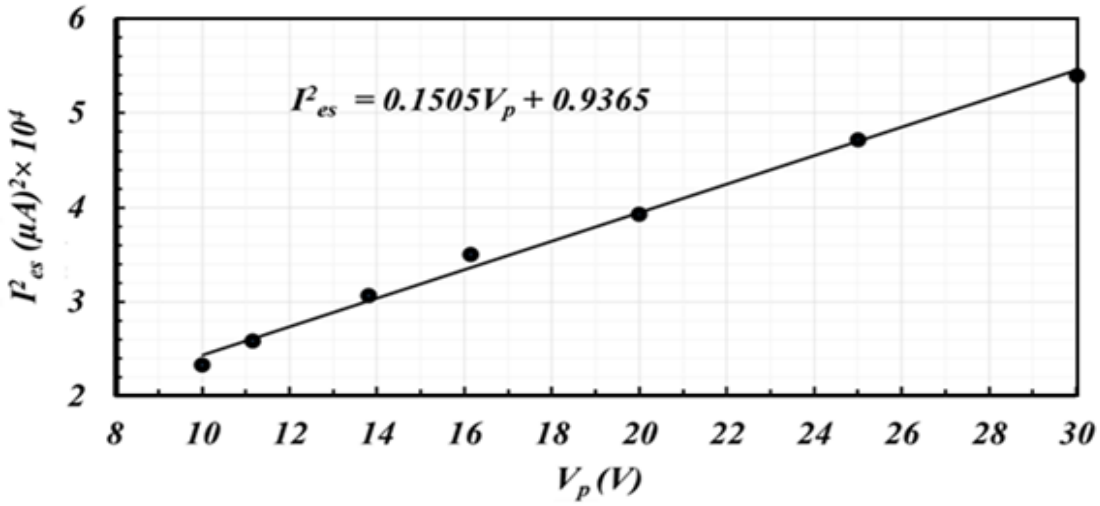

Fig. 5: Linear fitting for I^2_{es} as a function of the probe voltage V_P.

kg and $dI_e^2/dV_p = 1622 \times 10^{-8}$ A^2/V calculated in Fig. 5, the estimated value of the electron density using this region of the ($I_e - V_P$) curve, is $n_e \cong 2.90 \times 10^{13}$ m^{-3}. This value is nearly 40% lower than the value found in Section 3.2.1 above. Experimentally, it is not recommended to relay on the measurement of n_e using the electron saturation current, as given here. It can be quite inaccurate in a dense plasma and could draw drastically large probe currents. Generally, the determination of n_e from electron saturation current is unreliable and risky [14].

3.2.3 Ion Saturation Current I_{ion} [I – Squared Method]

The ion saturation current approach of calculating the electron density n_e is easier to manage and much accurate than the other approaches. The concentration of electrons can easily be obtained without the need to determine accurate value of the space or the plasma potential V_S or the electron temperature T_e. Equation (9) predicts that I^2_{ion} should vary linearly with the probe potential V_P, giving a

straight-line plot as shown in Fig. 6, from which n_i can be calculated. Using the simplified Eq. (12):

$$n_i \cong \frac{1.42 \times 10^{15}}{A_{P\,(m^2)}} \sqrt{m_i\,(\text{amu})\left(-\frac{dI_i^2}{dV_p}\right)} \qquad m^{-3}$$

with m_i = 40 amu for *Ar*-ions, A_P = 25.83 ×10^{-6} m^2 and dI_i^2/dV_p = – 0.177 ×10^{-12} A^2/V, result in n_i = 1.46 ×10^{14} m^{-3} = 1.46 ×10^8 cm^{-3} which is almost two times higher than the previously calculated value in section 3.2.1, using the electron current for $V_p < V_s$. Experimental results of n_i, obtained by several authors which have been summarized by Tichy and Smith [22, 23], showed that the values of the electron density (n_e) and the positive-ion density (n_i) deduced from the slope of the above plot of Fig. 6, were not equal; n_i always exceeding n_e and expressed empirically to it via the mass of the positive ion m_i (in amu) as: $n_i = (1 + 0.07\sqrt{m_i})n_e$. Our result suggests that the two values of (n_i) and (n_e) found in Sections 3.2.3 and 3.2.1 above, can be closely related as: $n_i = (1 + 0.154\sqrt{m_i})n_e$. Considering the quasi-neutrality of the plasma, such that $n_i \cong n_e$, and the value T_e = 2.48 eV in Eq. (14), then Debye length $\lambda_D \cong 0.97$ mm. Therefore, the ratio $\xi = r_P/\lambda_D \cong 1.19$ and it is expected that the sheath edge around the probe is not very thick and essentially very close to the area of the probe tip itself. The dependence of $I_i^2 \sim V_P$ is a clear indication of the validity of OML theory in explaining the results of this work with low electron density [21]. This value of λ_D agrees with the analytic fits (lines) for the computed data given by Laframboise in which the (I–V) curve approach the OML limit $I_i^2 \sim V_P$ as the ratio $\xi = r_P/\lambda_D$ gets smaller and the ion current I_i grows with increasing V_P as the sheath radius increases. Therefore, as long as the ion current I_i follows OML limit, then the value of the ion density $n_i \cong 1.46 \times 10^{14}$ m^{-3}, found from this approach is much more trustworthy than the previous value of the electron density $n_e \cong 7.4 \times 10^{13}$ m^{-3} calculated using the electron current approach above [14,18].

3.2.4 The Floating Potential - Child-Langmuir Method of Measuring Ion Density [FP − CL Method]

Following the work of Chen [14, 21, 24], in which a simple method for analyzing cylindrical Langmuir probe curves in a cold-ion plasma is described. The method is based on an extrapolation to the floating potential of the saturation ion current raised to the *4/3* power. If one assumes that the sheath thickness is given by the Child-Langmuir (C–L) law (neglecting the cylindrical curvature), the collection area expands as $V_p^{3/4}$, giving rise to the observed shape of the I–V curve. The ion current at the sheath edge is given by the Bohm sheath criterion for singly charged ions as:

$$I_i = 0.61\, n_i A_S (T_e \frac{e^3}{m_i})^{1/2} \qquad (18)$$

In Eq. (18), A_S represents the area of the sheath at the floating potential V_f, given by $A_S = 2\pi(r_P + d)L$, where r_P and L are the probe radius and length of the probe respectively and d is the sheath thickness with the factor (0.61) for Bohm coefficient [21]. In Fig. 7, the ion part of the (I–V) characteristic curve is raised to the *4/3* power and plotted against V_P, and a straight line is fitted to the part of the curve that is not affected by electron current. This straight line is extrapolated to V_f, where $I_p = I_{ion} - I_e = 0$, and gives an estimate of I_{ion} (V_f). The $V^{3/4}$ dependence of I_{ion} is reminiscent of the Child-Langmuir law for space-charge-limited emission, (C–L) law for pure ion sheaths, which is given by [14]:

$$J_{ion} = \frac{I_{ion}}{A_{sheath}} = \frac{4}{9}\,(\frac{2e}{m_i})^{1/2}\,\varepsilon_o\,\frac{|V - V_S|^{3/2}}{d^2} \qquad (19)$$

As shown in Fig. 7, the intersection of the line with the vertical line at floating potential V_f, yields the value of I_{ion} (V_f) = 1.2 µA used in the analysis. Using the value of V_f = – 2.2V, V_S = 6.1 V and $A_S = 2\pi(r_P + d)L$, then Eq. (19) can be solved for (d), such that:

$$d^2 = 0.17A_S = 0.17[2\pi(r_P + d)L] \qquad (20)$$

Which is a quadratic equation whose solution is d. Using r_p =1.15 mm and L= 3 mm, we can estimate the value of $d \cong 4.13$ mm (which is about 4.5 λ_D) at V_f, from which we can find that $A_S \cong 99.5$ mm^2. From Eq. (18), we can write:

$$n_i = \frac{I_i(V_f)}{0.61\,A_{sheath}}\,(\frac{m_i}{e^3 T_e})^{1/2} \qquad (21)$$

Substituting for T_e = 2.26 eV, m_i = 6.68 × 10^{-26} kg, A_S = 99.5 mm^2 and $I_{ion}(V_f)$ = 1.2 µA, we find that $n_i \cong 5.3 \times 10^{13}$ m^{-3} .This value is lower than the one found using the ion saturation part given in sections 3.2.3 and surprisingly, it is close to the value calculated in section 3.2.1 using the electron retardation region [18]. The calculated value $n_i \cong 5.3 \times 10^{13}$ m^{-3}, depends critically on the absolute value of $|V_f - V_s|$. Both values of V_f and V_S are subjected to some experimental errors [7, 8].

3.3 The Probe Heating Flux Effect

Usually, the probe used is in direct contact with the plasma and it is expected that it will be exposed to a continuous electron and ion bombardment during the time of measurement, which may lead to erroneous results [25]. The probe tip is 3.0 mm long and 2.3 mm in diameter, which is made up of pure tantalum. Considering the electron saturation region of the I–V curve, the probe was biased to 30 V and the plasma potential to 6.1 V, so, the electrons energy is 23.9 eV when they arrive at the probe, and the heat power per unit area (P) on the probe tip is:

$$P = \frac{I_{es}V}{A_P} = \frac{230\times 10^{-6}}{25.83\times 10^{-6}} \times \ 23.9 = 212.8\, Watt/m^2 \quad (22)$$

Assuming, that the electron saturation current last for t = 30 min to complete one continuous run, then the heat on the probe tip Q can be estimated as:

$$Q=P.A_P.t=\left(212.8\frac{Watt}{m^2}\right)(\,25.83\,\times\, 10^{-6}m^2)(1800s) \cong 9.9\,J \quad (23)$$

The heat Q can be calculated as:

$$Q = mC\Delta T \quad (24)$$

Where, C =148.3 *J/kg.k*, is the specific heat of tantalum and the mass (m) of the probe tip with probe tip volume, $V = \pi r_P^2 L = 1.246 \times 10^{-8}$ m^3 , $m = \rho V = (16690$ kg/m^3) (1.246×10^{-8} m^3) = 2.07×10^{-4} kg, so, the probe temperature rise (ΔT) is:

$$\Delta T = \frac{Q}{mC} = \frac{9.9\,J}{(2.07 \times 10^{-4}\ \mathrm{kg})148.3\,\frac{J}{kg.k}} \cong 323 \quad (25)$$

Repeating the same steps for the ion current region for the same time interval t = 30 min, with I_{isat} = 2μA and V = 30V,

$$P = \frac{I_{is}V}{A_P} = \frac{2.0 \times 10^{-6}}{25.83 \times 10^{-6}} \times\ 30 = 2.3\, Watt/m^2$$

$$\Delta T = \frac{Q}{mC} = \frac{2.3\,J}{(2.07 \times 10^{-4}\ \mathrm{kg})148.3\,\frac{J}{kg.k}} \cong 74$$

Hence, the maximum rise in temperature is 397°C, which is much lower than the melting point of tantalum. Therefore, the heating flux effect on the probe tip, is not that effective during the course of this experiment. However, the probe voltage should not be increased to high values in attempts to get the electron or ion saturation regions otherwise; the measurements must be performed within a very short time.

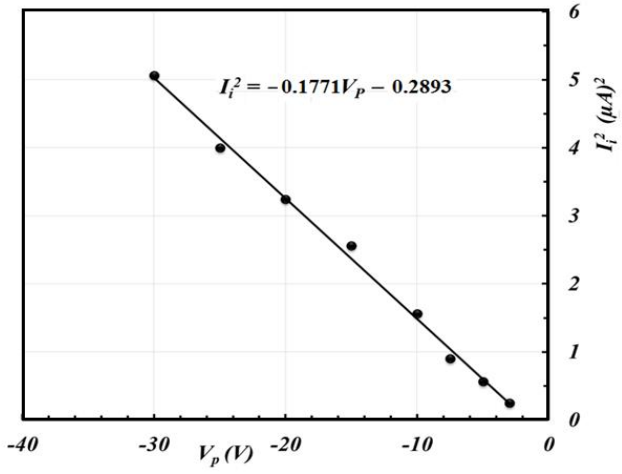

Fig. 6: Linear fitting for I^2_{ion} as a function of the probe voltage V_P.

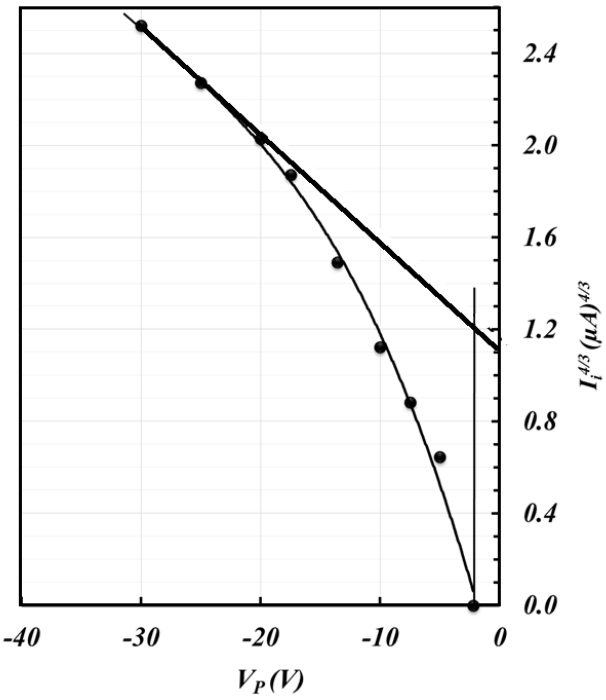

Fig. 7: Ion current $I_{ion}^{4/3}$ vs. V_p, for pure *Ar*-plasma and a least-squares fitted straight line.

4 Conclusions

In this work, the I–V characteristic curves of *Ar* – plasma of Freeman type ion source were studied under constant low *Ar* pressure and low magnetic field B = 20 mT. These *I–V* characteristics were used to analyze the plasma parameters such as plasma potential, electron temperature and electron number density. Table 1, summarizes the results of the measurements done in this work. It has been found that the I_i^2 fits better to a straight line than does $I_i^{4/3}$ and yields better and rather reasonable agreement with the value of n_e found from the retardation electron part, as shown in Fig. 6. These results suggest that Langmuir's original OML theory works pretty well for a small value of the ratio $\xi_p \equiv r_P/\lambda_D$ and at very low *Ar* pressure (4.7×10^{-3} mbar ~ 3.5 mTorr), which also an indication that some ion orbiting is taking place. Using (FP – CL) method suggested by Chen [18], we found that the ion current index of 4/3, $I_i^{4/3}$, fits within a very small range of the probe voltage (7–10V), and the calculation of the ion density gives lower value of $n_i = 5.3 \times 10^{13}$ m^{-3}, which is of the same order of magnitude with reference to the other methods, but it is much lower than the value found from the ion saturation region. It is obvious that this approach does not work very well for the low density plasma ~ 10^7 cm^{-3} and low Ar pressure ~ 10^{-3} Torr.

Acknowledgement: This work is partially supported by the research funds of the department of physics, college of

science, university of Baghdad. We appreciate the help of Mr. Inees K. Fawzi during the ion source operation.

References

[1] H A Hamad, N F Ali and H M Farok J. Nucl. Ene. Sci. Power Generat. Technol., 41.

[2] Remus-Sorin Dobrea, Ilarion Mihaila and Gheorghe Popa Materials Science and Engineering., **B.178** 1311, 2013.

[3] K S Jacobsen, J E Wahlund and A Pedersen Planetary and Space Science., **57**, 48, 2009.

[4] A Palmero, E D van Hattum, H Rudolph and F H P M Habraken Thin Solid Films., **494**, **18**, 2016.

[5] C Li, J H Hsieh, K L Huang, Yu Ting Shao and Yi Wen Chen Thin Solid Films., **544**, 37, 2013.

[6] I H Hutchinson Principles of Plasma Diagnostics (Cambridge: Cambridge University Press)., **Ch3**, 70, 2005.

[7] V A Godyak and V I Demidov J. Phys. D: Appl. Phys., **44**, 233001, 2011.

[8] V A Godyak and B M Alexandrovich Journal of Applied Physics., **118**, 233302, 2015.

[9] P Ivanova, Tsv K Popov, M Dimitrova, E Benova, T Bogdanov, J Stöckel and R Dejarnac Acta Technica., 56 T71, 2011.

[10] Tsv K Popov, P Ivanova, M Dimitrova, J Kovacic, T Gyergyek and M Cercek Plasma Sources Sci. Technol., **21**, 025004, 2012.

[11] E D van Hattum PhD Thesis (University of Utrecht, Nederland)., 2007.

[12] N Hershkowitz Plasma Diagnostics Volume I (eds) O Auciello and D L Flamm (London: Academic Press) 113, 1989.

[13] F F Chen J. Appl. Phys., **36**, 675, 1965.

[14] F F Chen Plasma Sources Sci. Technol., **21**, 055013, 2012.

[15] R L Merlino Am. J. Phys.,**75**, 1078 , 2007.

[16] H M Mott-Smith and I Langmuir Phys. Rev., **28**, 727 1926.

[17] F F Chen Phys. Plasmas., **8**, 3029, 2001.

[18] F F Chen Plasma Sources Sci. Technol., **18**, 035012 2009.

[19] N V Joshy PhD Thesis (Cochin University of Science and Technology, Kerala, India) ., 2008.

[20] S Bose, M Kaur, P K Chattopadhyay, J Ghosh, Y C Saxena and R Pal J. Plasma Phys., **83**, 615830201 2017.

[21] F F Chen, J D Evans and D Arnush Phys. Plasmas., **9** 1449, 2002.

[22] M Tichy, P Kudrna, J F Behnke, C Csambal, S Klagge J. Phys. IV France., **7**, C4-397, 1997.

[23] D Smith and I C Plumb J. Phys. D: Appl. Phys., **6**, 196 1973.

[24] F F Chen, John D Evans and Wade Zawalski Plasma Sources Sci. Technol., **21**, 055002, 2012.

[25] Y H Xie, C D Hu, S Liu, S H Shong, C C Jiang and Z M Liu Fusion Engineering and Design., **85**, 64, 2010.